Available online at www.sciencedirect.com
SCIENCE DIRECT
International Journal of Multiphase Flow 32 (2006) 791–806
International Journal of Multiphase Flow
www.elsevier.com/locate/ijmulflow

Two-phase flow characteristics in gas–liquid microreactors

Severin Waelchli, Philipp Rudolf von Rohr *

Institute of Process Engineering, Sonneggstr. 3, ETH Zurich, 8092 Zurich, Switzerland

Received 24 January 2005; received in revised form 6 February 2006

Abstract

Multiphase chemical microreactors require a detailed knowledge of the flow conditions inside the reaction system. This paper reports flow visualization measurements of the two-phase gas–liquid flow pattern and the liquid velocity distribution inside liquid plugs of an intermittent flow. Rectangular cross-section silicon microchannels with hydraulic diameters between 187.5 and 218 μm are fabricated. Laser Induced Fluorescence (LIF) is used to determine the flow pattern. To analyze the influence of the liquid properties and the channel diameter on the two-phase flow pattern, we present flow regime maps using different channel geometries and fluids. A universal flow pattern map based on dimensional analysis is presented. In contrast to microchannel flows, a great number of correlations for flow characteristics for multiphase flow in (round) pipes with diameters >1 mm exist. We compare our experimental results from optical flow visualizations in microreactors with common flow correlations and regime maps for macro- and microchannels. The recirculation motion in the liquid segments of an intermittent gas–liquid flow is analyzed using micron-resolution particle image velocimetry (μPIV). The velocity distribution influences the mixing and the mass transport towards the reactive phase interface dealing with two-phase chemical reactions. For straight microchannels hardly any mass transport over the center line is quantified. For enhanced mixing geometrical adaptations are suggested.

Keywords: Microreactor; Flow pattern; Liquid velocity distribution

1. Introduction

Due to the ongoing progress in the manufacturing techniques of microstructures, microchemical devices have become relevant for several applications. Microchemical reactors are superior to common batch reactors in the use of a minimum amount of fluids, the high heat and mass transfer rates, which result in shorter reaction times. These facts allow, for example, the implementation of precise and reproducible chemical or biological analysis. For the design of microchemical devices, the characteristics of the single or multiphase flow inside the device have to be known. The physical properties of single-phase microfluidic systems (Ehrfeld et al., 2000) or of reactor concepts using two miscible or immiscible liquid phases (Kolb and Hessel, 2004; Losey et al., 2001) are well understood. In the case of real technical applications, mostly multi-phase systems

* Corresponding author.
E-mail address: vonrohr@ipe.mavt.ethz.ch (P. Rudolf von Rohr).

0301-9322/$ - see front matter © 2006 Elsevier Ltd. All rights reserved.
doi:10.1016/j.ijmultiphaseflow.2006.02.014

can be found (chemical reactions as hydrogenations or fluorinations (de Mas et al., 2003), evaporation, condensation, etc.). For the design, the development and the operation of microscale chemical applications a detailed specific knowledge of the multi-phase flow and its properties as the flow pattern, the volumetric gas content, the pressure drop, the liquid film thickness or the internal mixing quality is of utmost importance.

The two-phase flow properties for circular (macroscale) pipes of diameters >1 mm are well known (Baker, 1954). In channels with diameters above some millimeters, the flow pattern is dominated by the influence of the gravitational force. In microchannels with diameters below some 100 μm, the flow pattern is mainly a function of the interfacial tension, the viscosity and the wall friction force. Only a few experimental studies describing the two-phase gas–liquid flow characteristics of microchannel flows have been reported (Coleman and Garimella, 1999; de Mas et al., 2003; Kawahara et al., 2002; Triplett et al., 1999). Velocity measurements in microchannel were mostly investigated in single-phase flows (Meinhart et al., 1999; Santiago et al., 1998).

In this work the flow pattern of two-phase gas–liquid flow and the liquid velocity distribution in intermittent microchannel flows are analyzed. Furthermore, the properties of microchannel flows are compared with experimental results and predictions for macroscale and microscale channel flows from previous works. We present experimentally derived flow pattern maps for a variety of flow configurations and detailed experimental studies of the internal mixing (recirculation) in the liquid phase of an intermittent flow in a microchannel. The internal mixing is a important factor dealing with two-phase chemical reactions which take place at the phase interface.

2. Experimental setup

All the presented experiments were performed in microchannels etched in silicon wafers by deep reactive ion etching (DRIE). A glass wafer bonded onto the silicon wafer covers the channels. The surface roughness caused by the etching process, which is in the order of several nanometers, is negligible compared to the resolution of the etching mask used for the microchannels in this study (exposed transparency film). The resolution of the mask (12,000 dpi) leads to a surface roughness of $k_S = 2.1$ μm. The channels are of rectangular cross-section with 150 μm in depth and widths between 150 μm and 400 μm. This results in hydraulic diameters D_h

$$D_h = \frac{4 \cdot A}{2 \cdot d + 2 \cdot w} = 150 \ldots 218.2\ \mu\text{m}, \tag{1}$$

where A denotes the cross-sectional area of the channel, d is the channel depth and w the channel width.

The channels are of a T-shape. For a better mixing of the two fluids, a static mixer consisting of several round silicon pins of 50 μm diameter is implemented in the mixing zone. The mixing zone reduces the inlet zone (distance to fully developed flow pattern) whereas the flow regime itself is shown not to be changed by its existence (Fig. 1).

For the presented two-phase gas–liquid experiments pure de-ionized water, ethanol and aqueous glycerol solutions (10% and 20% glycerol mass fraction) as liquid phase and nitrogen as gas-phase were used (see Table 1). The experiments were carried out at room temperature ($T = 25$ °C).

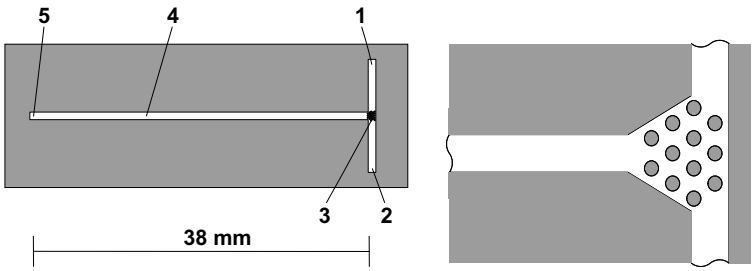

Fig. 1. Schematic of the rectangular T-shaped microchannel (left). The fluids entering through the liquid inlet (1) and the gas inlet (2) meet at the mixing zone (3) forming a two-phase flow pattern (4) and leave the channel through the outlet (5). Enlarged view of the mixing zone (right).

Table 1
Properties of the used fluids

Fluid	Density ρ [kg/m^3]	Viscosity η [mPa s]	Surface tension σ [N/m]
Deionized water	1000	1.002	0.073
Ethanol	790	1.190	0.022
Glycerol (10%)	1022	1.147	0.071
Glycerol (20%)	1046	1.555	0.073
Nitrogen	1.25	0.014	–

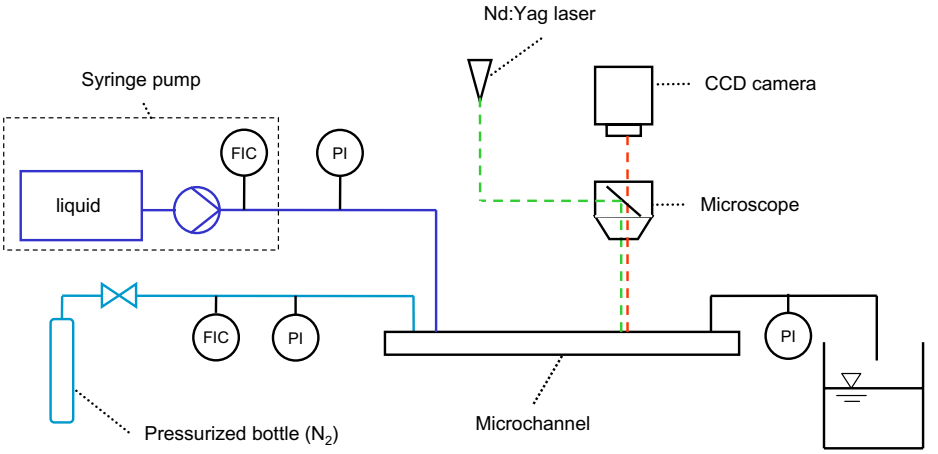

Fig. 2. Schematic of the optical measurement system. FIC stands for flow indicator and controller, PI for pressure indicator.

The liquid phase is dosed by a syringe pump (Harvard Apparatus, accuracy within 0.35% and reproducibility within 0.05%). The volumetric flow rate of the liquid phase, $\dot{V}_L$, is varied between 0.05 and 5 ml/min for the presented experiments. The gas-phase volumetric flow rate, $\dot{V}_G$, was controlled by a mass flow controller (Bronkhorst, accuracy ±0.5% of reading plus ±0.1% full scale) and is varied between 1 and 20 ml/min. The two flows are fed into the microchannels by flexible pipes (PEEK, 0.5 mm inner diameter, Vici AG International). Pressures are measured, at the inlet and outlet of the microchannel, by pressure sensors (Endress + Hauser, accuracy ±0.5%). The single-phase fluids meet in a mixing zone where the multiphase flow pattern is formed. The total length of the multiphase part of the microchannel is $l = 38$ mm, which corresponds to $174 \ldots 253 \cdot D_h$.

For the flow pattern and the velocity measurements, the multiphase two-component flow is recorded by a CCD camera (PCO SensiCam QE, 1376×1040 pixels, area of view 1.03 mm × 1.36 mm, spatial resolution 0.99 μm/pixel) through the optically transparent glass cover using an inverted fluorescence microscope (Carl Zeiss Axiovert 200). The measurement location was chosen at $l_m = 34$ mm from the mixing zone ($l_m/D_h \approx 156 \ldots 227$). The channel was illuminated by a 532 nm pulsed Nd:YAG laser (TSI) (Fig. 2).

3. Measurement methods

3.1. Flow pattern measurements using laser induced fluorescence (LIF)

The flow pattern experiments were carried out using the Laser Induced Fluorescence (LIF) technique. Rhodamine B was added to the water (0.5 ml of 25% solution into 50 ml liquid). Rhodamine B emits red light (600 nm) when excited by a 532 nm laser light. The liquid phase is therefore represented by bright colors on the grayscale images.

To obtain a flow pattern map, images of 120 combinations of liquid ($\dot{V}_L$) and gas ($\dot{V}_G$) flow rates were recorded. According to Coleman and Garimella (1999), we differentiated the four major flow regimes, including stratified, intermittent, annular and bubbly/dispersed flow (see Table 2). The Bond number in this work is

Table 2
Flow regime classifications according to Coleman and Garimella (1999)

Major flow regime	Flow patterns
Stratified	Stratified smooth Stratified wavy
Intermittent	Elongated bubble (plug) Slug flow
Annular	Wavy annular Annular
Bubbly	Bubbly flow Dispersed flow

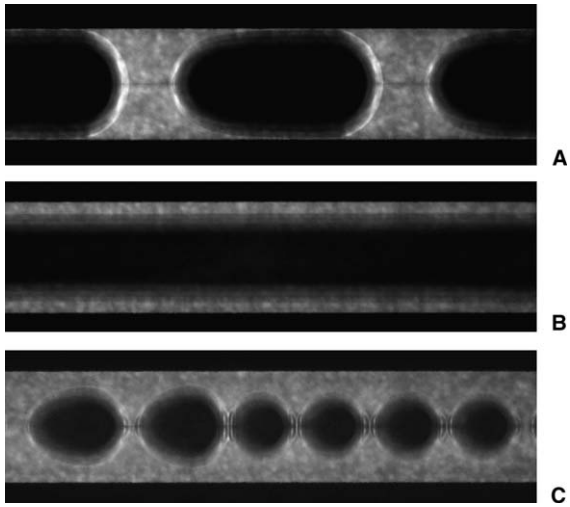

Fig. 3. Description of flow regimes in the present experiments. A: intermittent flow, B: annular flow, C: bubbly flow.

$Bo \cong 5 \times 10^{-3}$. According to the agreement on a limiting value of the Bond number exceeding 0.15 to allow occurrence of stratified flow, this flow pattern is not detected in this work.

Flow regime description:

- Intermittent flow (see Fig. 3A): Characterized by discontinuities in the liquid and gas flow. Only a thin film of liquid coats the wall surrounding the gas phase plug. Slug and plug flow are combined in the intermittent flow regime.
- Annular flow (see Fig. 3B): The annular flow pattern is defined by a flowing gas core surrounded by the liquid phase pushed up around the circumference of the channel walls.
- Bubbly flow (see Fig. 3C): The flow pattern was associated with bubbly flow, when the gas phase, in the microchannel, was of circular shape in the 2-dimensional images and not taking more than 80% of the channel cross-section at the point of the largest gas bubble diameter. In contrast to the intermittent flow regime, at least the two smaller walls of the microchannel are not only covered by a liquid film anymore, but by a larger amount of liquid.

3.2. Liquid velocity measurements using microparticle image velocimetry (μPIV)

For the measurement of the velocity distribution inside the liquid phase in intermittent flow patterns, micron-resolution particle image velocimetry (μPIV) was used. Therefore, red fluorescent polymer micro-

spheres with 1 μm mean diameter (Duke Scientific Corporation) were added to the liquid. The velocity components are computed by the standard cross-correlation routine (Flowmaster, LaVision). Due to the fact that intermittent flow is a non-stationary flow pattern, averaging the velocity components of the complete area of view of the CCD camera over a large amount of images was not possible. An area of interest (master, see Fig. 4) was manually chosen in one image.

For each full-scale raw image, a cross-correlation routine searches the section of the same size as the master with the best conformance. The maximum of the correlation factor, $r[i,j,N]$, yields the position $[i,j]$ and the correlation value of the PIV image N with the master image. The values of the cross-correlation factors are

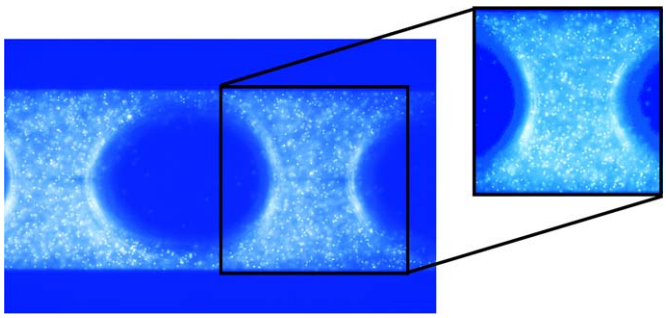

Fig. 4. Manually chosen area of interest (master) in a recorded PIV-image of a particle seeded flow in a rectangular microchannel of 400 μm width.

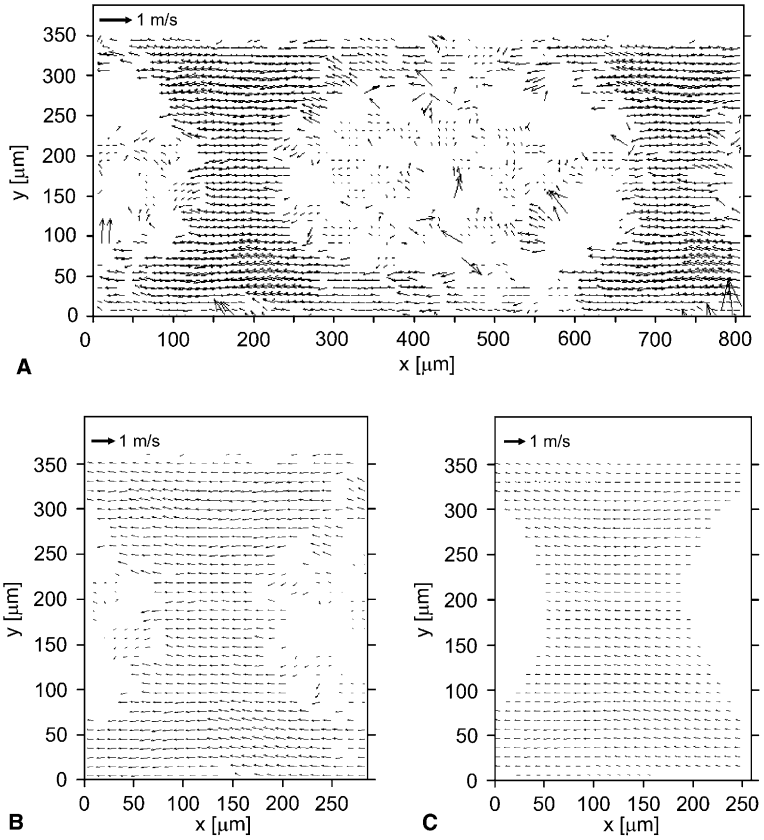

Fig. 5. Raw velocity field of complete area of view (1376 × 1040 pixels) in rectangular channel with $D_h = 210$ μm using ethanol as working fluid (A). Velocity field of extracted liquid plug (B). Averaged velocity field (250 images) (C).

normalized using the factor of the image, where the master is taken from. For this image, the cross-correlation factor is maximal and the normalized $r[i_{max},j_{max},N_{master}]_{norm}$ equals 1. For a further processing of each image, we defined a minimum cross-correlation factor of *0.80* to be required. With this value a misinterpretation or a wrongly identified liquid plug could be avoided.

For each recorded image N with a $r[i_{max},j_{max},N]_{norm} > 0.80$ the raw vector section of the same size as the master at the position $[i,j]$ (Fig. 5B) in the full scale velocity vector file (Fig. 5A) was extracted. For all the presented experiments 250 vector files are averaged (Fig. 5C).

4. Results and discussion

4.1. Flow pattern maps for rectangular shaped microchannels

Flow regime maps for two-phase flow in channels or pipes are used to predict the flow pattern. In most of the existing maps (Zhao and Bi, 2001; Triplett et al., 1999; Kawahara et al., 2002; Coleman and Garimella, 1999) the flow pattern is plotted as a function of the superficial gas and liquid velocities,

$$j_{G,L} = \frac{\dot{V}_{G,L}}{A}, \tag{2}$$

where A denotes the channel cross-section. Some flow regime maps use the gas and liquid flow rate as well as of some fluid properties of the two-phases as coordinates (Baker, 1954). Therefore most of the common flow pattern maps are valid for a specific combination of liquids, channel geometry (cross-sectional shape) and channel material only.

In the present study, flow pattern maps for two-phase gas–liquid flows in rectangular microchannels for several hydraulic diameters D_h and three different liquids were constructed. Deionized water features a viscosity similar to ethanol, $\eta_{water}/\eta_{eth} = 0.85$. The interfacial tension of water however is larger than the one of ethanol by a factor of $\sigma_{water}/\sigma_{eth} = 3.26$. The ratio of the surface tension between the aqueous 20% glycerol mixture and water is close to one, $\sigma_{water}/\sigma_{glyc} = 0.99$, the viscosity ratio on the other hand is much higher, $\eta_{glyc}/\eta_{water} = 1.54$ (see Table 3).

For each configuration (hydraulic diameter D_h, gas and liquid flow rate $\dot{V}_{L,G}$ and fluid combination) a sample of 50 images was taken. Especially in the transition regions (bubbly/intermittent, intermittent/annular), not a unique flow pattern was detected. According to the higher number of apparent flow regime the configuration was categorized. This circumstance clarifies that the transition boundaries in the presented flow pattern maps are transition regions more than sharp transition lines. In all the following figures, the present experimental data is plotted as follows:

- ● represents intermittent flow
- □ annular flow and
- △ bubbly flow regime

Fig. 6A–E show flow pattern maps for the different configurations mentioned above.

Apparently, the presented regime maps show different transition boundaries for any of the analyzed configuration. When designing a microreactor for a chemical gas–liquid reaction where a specific interfacial area is required, detailed knowledge of the according flow pattern and the flow rates is inevitable. By just changing the liquid phase from ethanol to water for example, the flow pattern maps presented above and the existing regime maps in the literature cannot be used anymore. Therefore, a more universally applicable flow regime map is desired. Due to the large number of influencing factors, a completely universal pattern map is unreal-

Table 3
Comparison of the properties of the fluids employed

Fluid combination	Surface tension ratio	Viscosity ratio
Water–ethanol	$\sigma_{water}/\sigma_{eth} = 3.26$	$\eta_{water}/\eta_{eth} = 0.85$
Water–glycerol (20%)	$\sigma_{water}/\sigma_{glyc} = 0.99$	$\eta_{glyc}/\eta_{water} = 1.54$

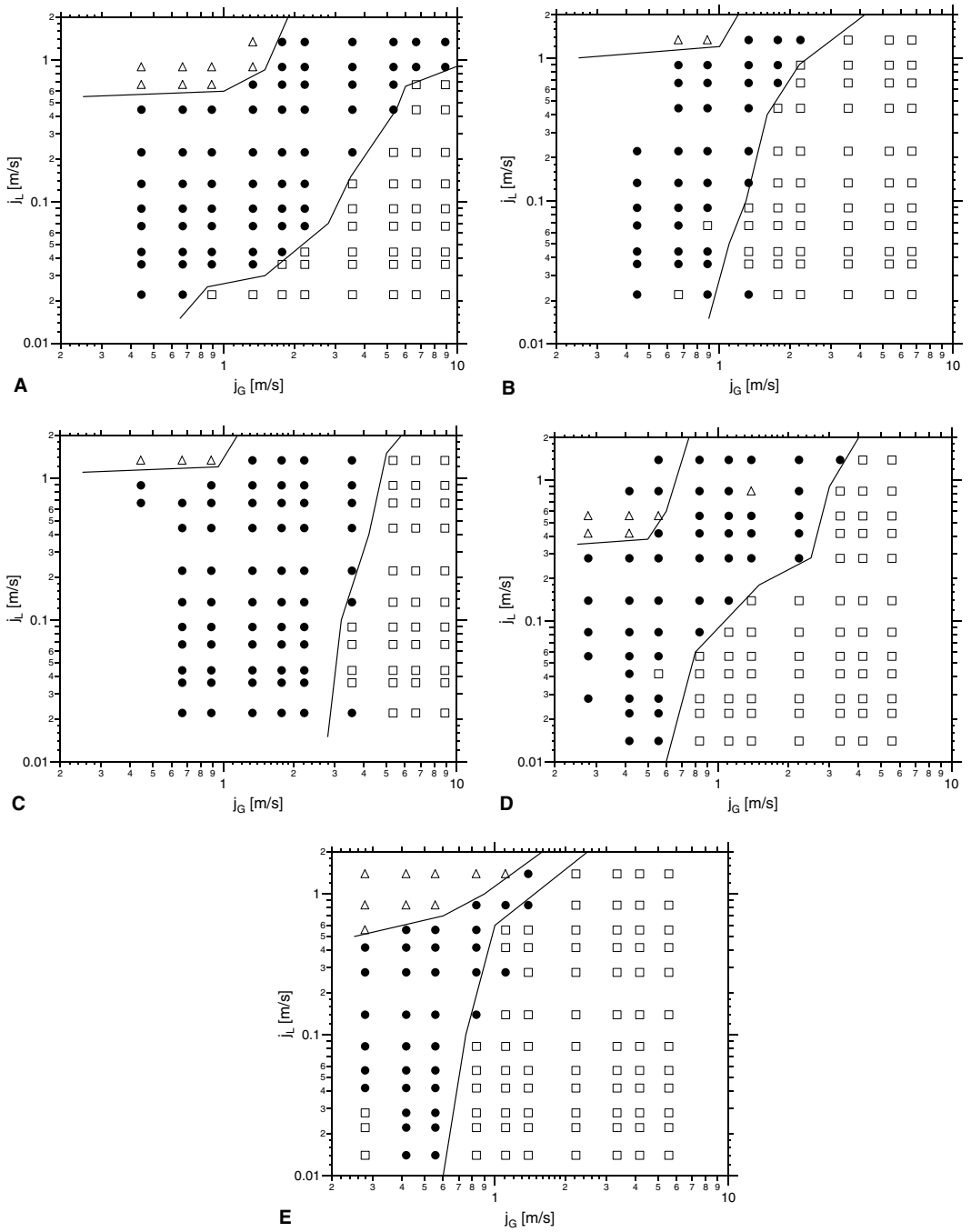

Fig. 6. Flow pattern maps in a rectangular microchannel with a hydraulic diameter $D_h = 187.5$ μm using water–nitrogen (A), ethanol–nitrogen (B) and glycerol–nitrogen (C), respectively. The same fluid configuration (D: water–nitrogen, E: ethanol–nitrogen) were analyzed in a channel with $D_h = 218$ μm.

istic. Besides the fluid properties and the hydraulic diameter of the channel varied in the present study, also the channel material, its surface roughness, the cross-sectional shape and other variables as temperature or the applied pressure are influencing the appearing flow pattern.

Taking into account the fluids kinematic viscosities, $v_{L,G}$, their surface tension, σ, the difference of the fluid densities, $\Delta\rho$, the superficial velocities, $j_{L,G}$, the hydraulic diameter, D_h, and the channel roughness, k_S,

Table 4
Dimension matrix of the influencing factors according to Buckingham (1914) and Zlokarnik (1983)

	Core matrix			Remnant matrix				
	ρ	D_h	σ	j_L	j_G	v_L	v_G	k_S
Mass M [kg]	1	0	1	0	0	0	0	0
Length L [m]	−3	1	0	1	1	2	2	1
Time T [s]	0	0	−2	−1	−1	−1	−1	0

Table 5
Dimension matrix after transfer into a unit matrix by linear transformations

	Unit matrix			Remnant matrix				
	ρ	D_h	σ	j_L	j_G	v_L	v_G	k_S
$M+\frac{1}{2}T$	1	0	0	$-\frac{1}{2}$	$-\frac{1}{2}$	$-\frac{1}{2}$	$-\frac{1}{2}$	0
$(L+3M)+\frac{3}{2}T$	0	1	0	$-\frac{1}{2}$	$-\frac{1}{2}$	$\frac{1}{2}$	$\frac{1}{2}$	1
$-\frac{1}{2}T$	0	0	1	$\frac{1}{2}$	$\frac{1}{2}$	$\frac{1}{2}$	$\frac{1}{2}$	0

universal flow regime transition boundaries (universal flow pattern map) are presented for silicon microchannels with rectangular cross-section. All the experiments were conducted at room temperature, so the influence of changes in fluid properties by a change in temperature was not examined, as well as changes in the cross-sectional shape of the microchannel. For the reduction of the above mentioned influencing factors, the Buckingham Π-theorem (Buckingham, 1914; Zlokarnik, 1983) was used.

Table 4 shows the dimension matrix constructed for the influencing parameters. This table is structured in a core matrix and a remnant matrix.

The core matrix is transferred into a unit matrix by linear transformations (see Table 5).

This matrix analysis leads to the remaining five characteristic numbers, Π_1 to Π_5.

$$\begin{aligned}
\Pi_1 &= \frac{j_L}{\Delta\rho^{-\frac{1}{2}}\cdot D_h^{-\frac{1}{2}}\cdot\sigma^{\frac{1}{2}}} = \frac{j_L\cdot\Delta\rho^{\frac{1}{2}}\cdot D_h^{\frac{1}{2}}}{\sigma^{\frac{1}{2}}},\\
\Pi_2 &= \frac{j_G}{\Delta\rho^{-\frac{1}{2}}\cdot D_h^{-\frac{1}{2}}\cdot\sigma^{\frac{1}{2}}} = \frac{j_G\cdot\Delta\rho^{\frac{1}{2}}\cdot D_h^{\frac{1}{2}}}{\sigma^{\frac{1}{2}}},\\
\Pi_3 &= \frac{v_L}{\Delta\rho^{-\frac{1}{2}}\cdot D_h^{\frac{1}{2}}\cdot\sigma^{\frac{1}{2}}} = \frac{v_L\cdot\Delta\rho^{\frac{1}{2}}}{D_h^{\frac{1}{2}}\cdot\sigma^{\frac{1}{2}}},\\
\Pi_4 &= \frac{v_G}{\Delta\rho^{-\frac{1}{2}}\cdot D_h^{\frac{1}{2}}\cdot\sigma^{\frac{1}{2}}} = \frac{v_G\cdot\Delta\rho^{\frac{1}{2}}}{D_h^{\frac{1}{2}}\cdot\sigma^{\frac{1}{2}}},\\
\Pi_5 &= \frac{k_S}{D_h}.
\end{aligned} \tag{3}$$

A transformation of these five characteristic numbers results in a set of necessary dimensionless numbers $\{Re_G, Re_L, We_G, We_L, \frac{k_S}{D_h}\}$ to fully characterize the transition lines.

$$\begin{aligned}
\Pi_1^2 &= \frac{j_L^2\cdot\Delta\rho\cdot D_h}{\sigma} = We_L,\\
\Pi_2^2 &= \frac{j_G^2\cdot\Delta\rho\cdot D_h}{\sigma} = We_G,\\
\Pi_1\cdot\Pi_3^{-1} &= \frac{j_L\cdot D_h}{v_L} = Re_L,\\
\Pi_2\cdot\Pi_4^{-1} &= \frac{j_G\cdot D_h}{v_G} = Re_G,\\
\Pi_5 &= \frac{k_S}{D_h},
\end{aligned} \tag{4}$$

where the Reynolds number

$$Re_{L,G} = \frac{j_{L,G} \cdot D_h}{\nu_{L,G}} \tag{5}$$

implies the impact of the hydraulic diameter, the superficial velocity and the fluid viscosity, whereas the Weber number

$$We_{L,G} = \frac{\Delta\rho \cdot j_{L,G}^2 \cdot D_h}{\sigma} \tag{6}$$

is used to include the influence of the fluid densities and the surface tension.

The dimension analysis state that there is a function f valid for the regime transition boundaries (tb), where

$$f\left(Re_G, Re_L, We_G, We_L, \frac{k_S}{D_h}\right)_{tb} = 0. \tag{7}$$

As transition boundaries (tb) the conditions of flow pattern changes from annular flow to intermittent flow and from intermittent flow to bubbly flow (transition lines in Figs. 6A–E) are considered.

Eq. (7) is the maximum information the dimension analysis is able to provide. The exact form of the function f can only be extracted from experimental results. In most cases, f is an exponential function. For the universal flow pattern transition boundaries in the present study, we used

$$\left[a \cdot Re_L^b \cdot We_L^c \cdot \left(\frac{k_S}{D_h}\right)^d\right]_{tb} = [Re_G^e \cdot We_G^f]_{tb}. \tag{8}$$

A parameter variation for the parameter a, b, c, d, e and f, using a least square fit of data points of both transition lines (annular-intermittent and intermittent-bubbly) yielded the exponents found in Table 6. The improved quality of two separate sets of exponents for the two transition boundaries, thinking of the large number of additional (not considered) influences, is negligible. Hence for practical reasons we concentrated on a single set of exponents for both transition lines, as they can be plotted in the same graph (Fig. 7).

According to the results of the parameter variation for the transition boundaries,

$$Re_G^{0.2} \cdot We_G^{0.4} \tag{9}$$

of all the experimental data points (x-axis) is plotted versus

$$10^7 \cdot Re_L^{0.2} \cdot We_L^{0.4} \cdot \left(\frac{k_S}{D_h}\right)^5. \tag{10}$$

For all the presented experimental data, the universal flow pattern transition boundaries show a satisfying agreement. The two boundary lines are located in the transition regions for all the experimental data. Therefore the universal flow pattern map is capable to make a prediction of the expected flow pattern for a large variety of fluid and geometrical conditions.

Looking at Eq. (11), it can be seen, that the axes of the universal flow pattern map are proportional to the superficial gas and liquid velocities, respectively. The regime map is therefore consistent with other flow pattern maps found in the literature. The additional factors are used for the adaptation for different fluid properties and channel diameters.

$$Re_{G,L}^{0.2} \cdot We_{G,L}^{0.4} = (Re_{G,L} \cdot We_{G,L}^2)^{0.2} = j_{G,L}\left(\frac{D_h^3 \cdot \Delta\rho^2}{\nu_{G,L} \cdot \sigma^2}\right)^{0.2} \sim j_{G,L}. \tag{11}$$

Table 6
Exponents for universal flow pattern transition boundaries according to Eq. (8)

Exponent	a	b	c	d	e	f
Value	10^7	0.2	0.4	5	0.2	0.4

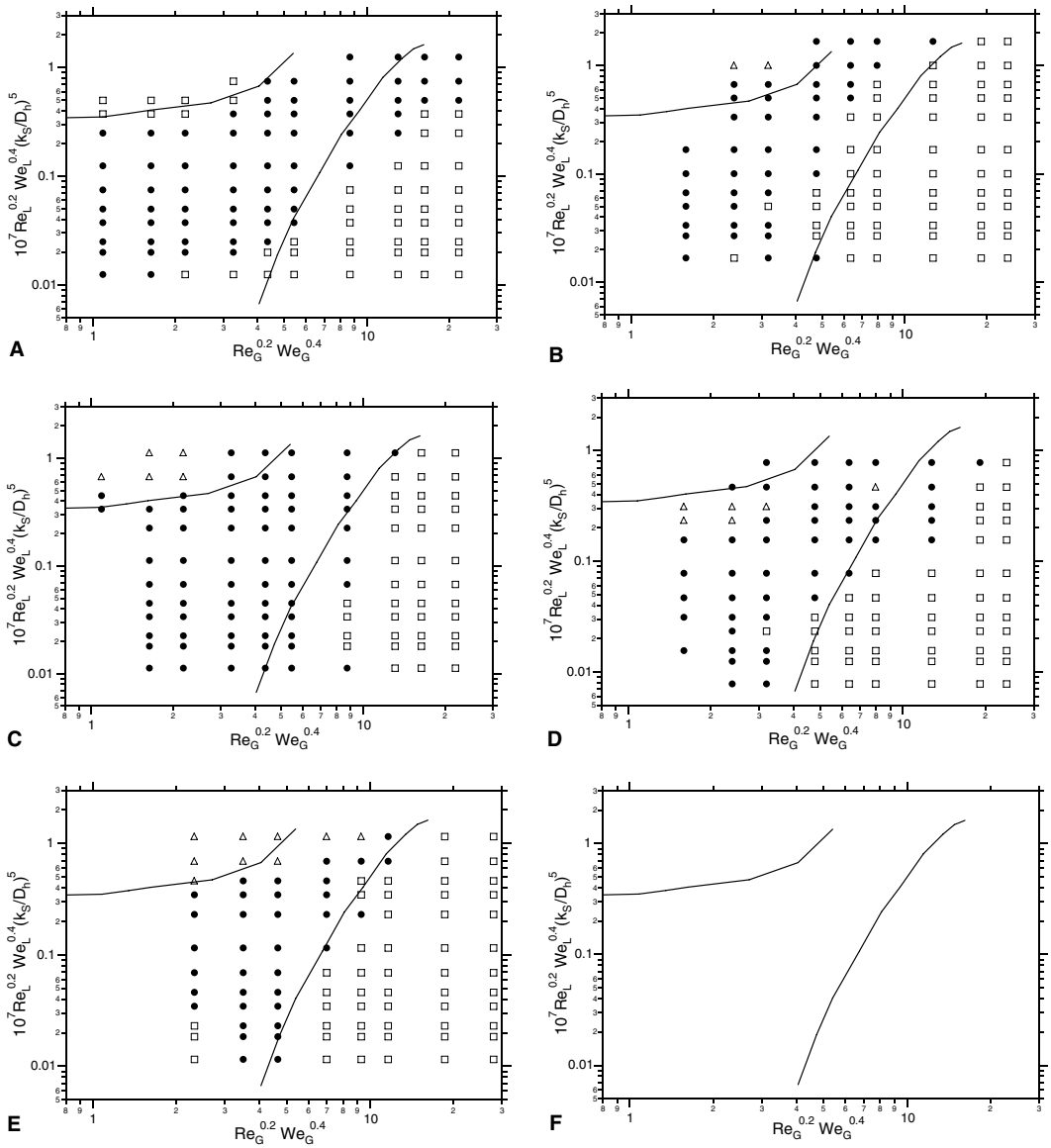

Fig. 7. Flow pattern maps using the universal pattern transition boundaries (F) for a rectangular microchannel for the same flow and geometry conditions as in Fig. 6 (A: water, $D_h = 187.5$ μm; B: ethanol, 187.5 μm; C: glycerol, 187.5 μm; D: water, 210 μm; E: ethanol, 210 μm).

The fact that additional important influencing factors as temperature, the cross-sectional shape or the channel material and surface roughness, were not varied or neglected in the presented flow regime map, shows the indispensable need for the experimental verification of the flow pattern for the detailed design of a chemical microreactor.

4.2. Comparison with existing flow pattern maps

Our experimentally derived pattern map for the microchannel with a hydraulic diameter of $D_h = 210$ μm using water and nitrogen as working fluids was compared to several existing flow regime maps. Flow maps to which our results are compared are selected carefully from the large range of existing maps. Among the selection criteria were similar dimensions, similar substance properties, recent publications, range of Bond number.

4.2.1. Flow regime map by Baker (1954)

Due to the fact that the flow pattern map by Baker (Fig. 8A) bases on flow through large diameter pipes ($D_h \gg 210$ μm), an accurate consistency of the flow regime cannot be expected. The experimental data is shifted towards lower gas flow rates. For the Baker flow regime map, no weighting factors are present to adapt

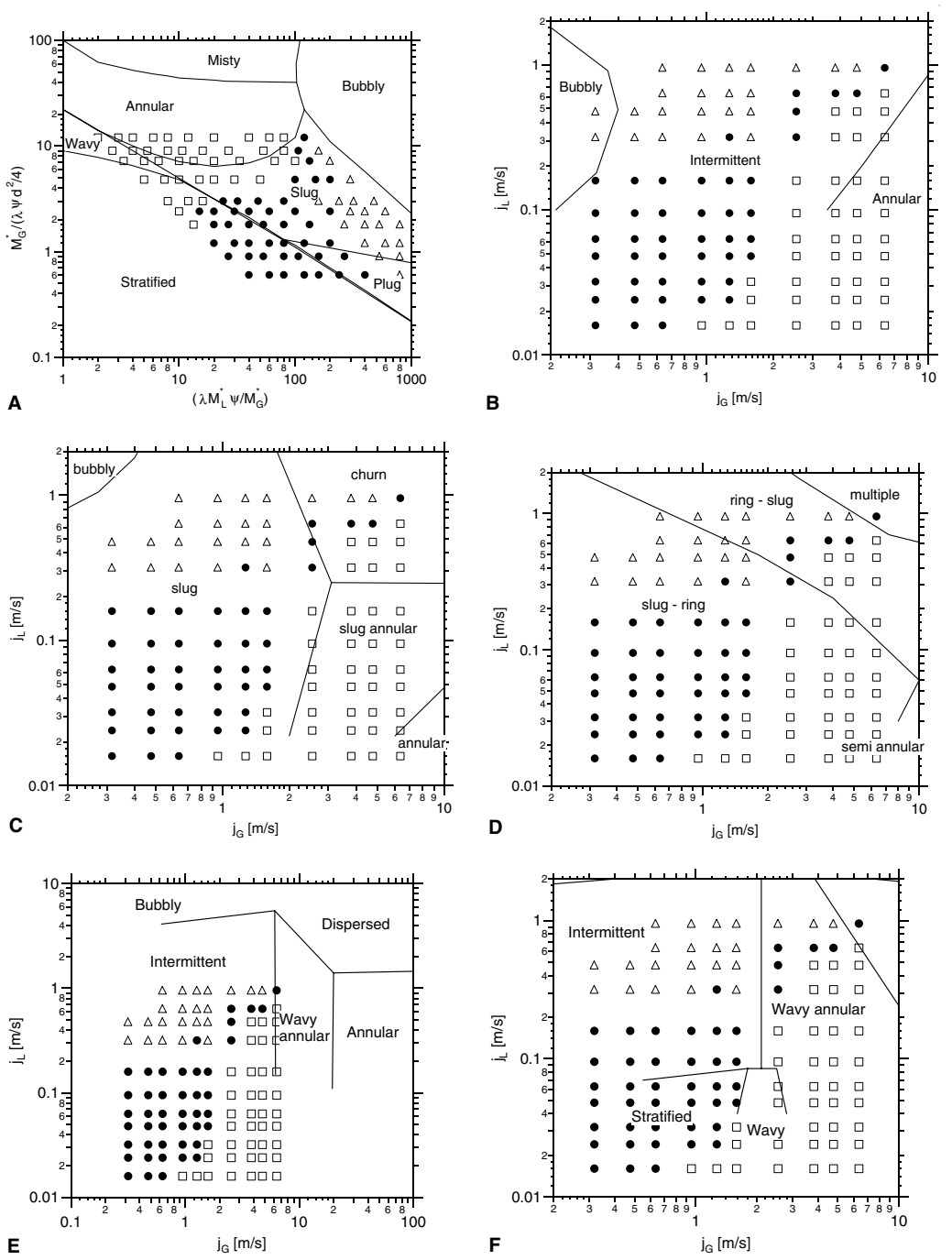

Fig. 8. Two-phase flow regime maps of several authors using water as working fluid compared with the present experimental data of a rectangular microchannel with a hydraulic diameter $D_h = 210$ μm (A: Baker, circular; B: Zhao, triangular, 0.866 mm; C: Triplett, semi-triangular, 1.09 mm; D: Kawahara, circular, 100 μm; E: Coleman, circular, 1.30 mm; F: Coleman, rectangular, 5.36 mm).

the transition boundaries to the phenomena in microchannels. The Baker diagram therefore is not capable to predict accurately flow pattern for microfluidic applications.

4.2.2. Flow pattern map by Zhao and Bi (2001)

The flow regime map of Zhao (Fig. 8B) is experimentally derived using an air–water mixture in triangular microchannels with a hydraulic diameter of $D_h = 866$ μm. This hydraulic diameter is still larger than the diameters in the present study by a factor of approximately 4. The agreement between the present data and the regime map for the microchannel by Zhao is accurate for the flow pattern change between intermittent (slug) and annular flow. Due to the larger hydraulic diameters and the different channel geometry, no bubbly flow was detected at higher superficial gas velocities.

4.2.3. Flow regime map by Triplett et al. (1999)

The results of Triplett (Fig. 8C) are based on experiments using air and water as fluids in semi-triangular microchannels of hydraulic diameters $D_h = 1.09$ mm. Even though the hydraulic diameter and the cross-sectional shape of the channels are similar to the ones in the experiments by Zhao, the flow regime map by Triplett predicts the flow patterns of the two-phase flow in microchannels of rectangular cross-section and hydraulic diameters smaller by a factor of 5 with high accuracy. Again, no bubbly flow was detected.

4.2.4. Flow pattern map by Kawahara et al. (2002)

Kawahara used de-ionized water and nitrogen as working fluids and circular microchannels with an inner diameter $D = 100$ μm. Even though the hydraulic diameters of the present study are the closest to those shown by Kawahara, the data does not correspond. The transition between the slug and the annular flow regime seems to be shifted towards smaller superficial gas velocities (Fig. 8D).

4.2.5. Flow regime map by Coleman and Garimella (1999)

Coleman carried out some of the experiments in round tubes with an inner diameter of $D = 1.30$ mm, others in microchannels of rectangular cross-section with a hydraulic diameter of $D_h = 5.36$ mm. The used fluids are air as gas-phase and water as liquid-phase. Fig. 8E shows the comparison of the present data with the flow regime map for the circular channel and Fig. 8F for the rectangular microchannel by Coleman. The consistency with the circular channel is insufficient even though the hydraulic diameter is closer to the ones in the present experiments. All the data points are in the intermittent (plug and slug) flow regime even though annular flow was detected in the present experiments.

The agreement with the regime map obtained in the rectangular microchannel is accurate. Again, no bubbly flow is predicted for the larger channel. The impact on the flow regime by the cross-sectional shape of the microchannel seems to be more important than by the hydraulic diameter. The ratio between the hydraulic diameter by Coleman and the present study is

$$\frac{D_{h,\mathrm{Coleman}}}{D_{h,\mathrm{present}}} = \frac{5.36}{0.210} = 25.5. \tag{12}$$

4.3. Liquid velocity distribution

The velocity distribution inside the liquid plug of a gas–liquid two-phase intermittent flow is an important factor of the internal mixing (recirculation) in chemical microreactors. The recirculation determines the mass transfer to the phase interface and therefore influences the reaction rate of a chemical gas–liquid reaction. The mixing quality is mainly dependent on the fluid velocities, their properties and the channel geometry, which includes not only the reactor shape and hydraulic diameter, but also the surface roughness.

In the present study we experimentally determined the liquid velocity distribution in intermittent flow in straight microchannels of rectangular cross-section with low superficial liquid velocities. Three different liquids are used, deionized water, ethanol and a 10% aqueous glycerol mixture. The properties of the liquids can be found in Table 1. Nitrogen was used as the gas phase in all cases.

The internal recirculation was analyzed for different flow conditions and hydraulic channel diameters. Using a liquid flow rate of 0.1 ml/min, a gas flow rate of 1.0 ml/min and a microreactor with a hydraulic diameter of $D_h = 210$ μm, yielded in a superficial liquid velocity of $j_L = 0.032$ m/s and a superficial gas velocity of $j_G = 0.317$ m/s. According to the flow pattern maps presented in Section 4.1 intermittent flow is apparent. Using water as liquid, these flow conditions are represented by Reynolds numbers of

$$Re_L = \frac{j_L \cdot D_h}{v_L} = 7.45, \quad Re_G = \frac{j_G \cdot D_h}{v_G} = 4.31. \tag{13}$$

Fig. 9A shows the velocity distribution inside the liquid water plug of the intermittent flow. The average liquid velocity is 0.36 m/s. To investigate the amount of mixing and the mass transport towards the phase interfaces, which are the reaction interfaces in microchemical gas–liquid reactions, the relative velocities

$$v_{rel} = v_{abs} - v_{average} \tag{14}$$

are plotted in Fig. 9B, where v_{abs} are the measured absolute velocities and $v_{average}$ is the mean velocity. Two counter-rotating vortices are observable. In the center of the microchannel low velocities are present and hardly any mass transfer over the center line is determinable. The velocity distribution is symmetric.

Ethanol has a higher viscosity and a much lower surface tension than water (see Table 1). Using the same flow conditions as in the water case ($j_L = 0.032$ m/s and $j_G = 0.317$ m/s), the liquid Reynolds number drops to $Re_L = 4.94$ using ethanol as the liquid phase. The average velocity inside the plug increases to $v_{average} = 0.38$ m/s. The ethanol plug length is slightly smaller than the water plug. The absolute velocity distribution (Fig. 10A) shows similar characteristics as the ones using water, whereas the relative velocities (Fig. 10B) behave remarkably different. Comparatively large velocities are measured throughout the liquid plug. The typical vortices are more distinctive, the stagnation points in the liquid phase close to the leading and the trailing end of the gas phase found in the water case are hardly identifiable. The velocities at the center line are larger.

Further experiments of the liquid properties on the velocity distribution inside the liquid plug were performed using an aqueous glycerol solution as liquid phase. This fluid is characterized by a viscosity similar to ethanol ($v_{glyc} = 1.14$ mPa s, $v_{eth} = 1.190$ mPa s) and a value for the interfacial tension against nitrogen similar to water ($\sigma_{glyc} = 0.07336$ N/m, $\sigma_{water} = 0.07275$ N/m). These properties yield in a liquid Reynolds number of $Re_L = 6.64$. The average velocity of the liquid plug is lower than in the two cases presented above, $v_{average} = 0.22$ m/s. This can also be seen in the distribution of the absolute velocity distribution in Fig. 11A. However, the distribution of the relative velocities resembles the ones found using water as liquid. Low relative velocities and two stagnation points at the center line are significant.

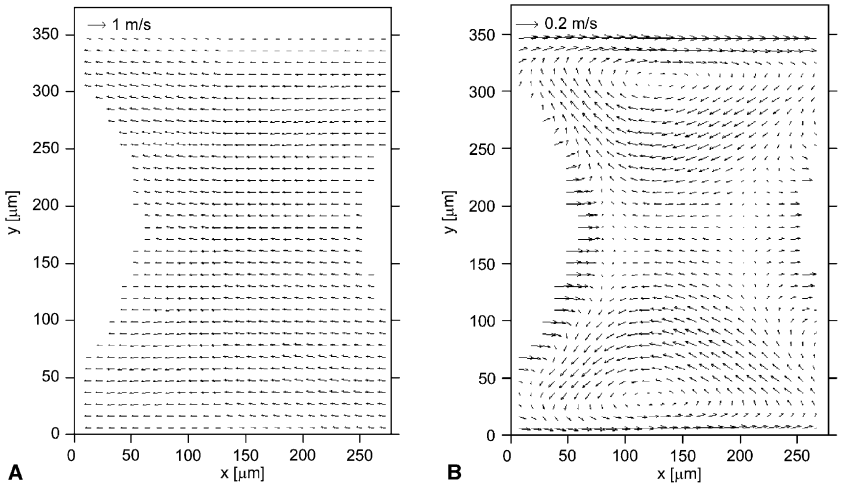

Fig. 9. Distribution of the absolute (A) and relative (B) velocities inside a water plug.

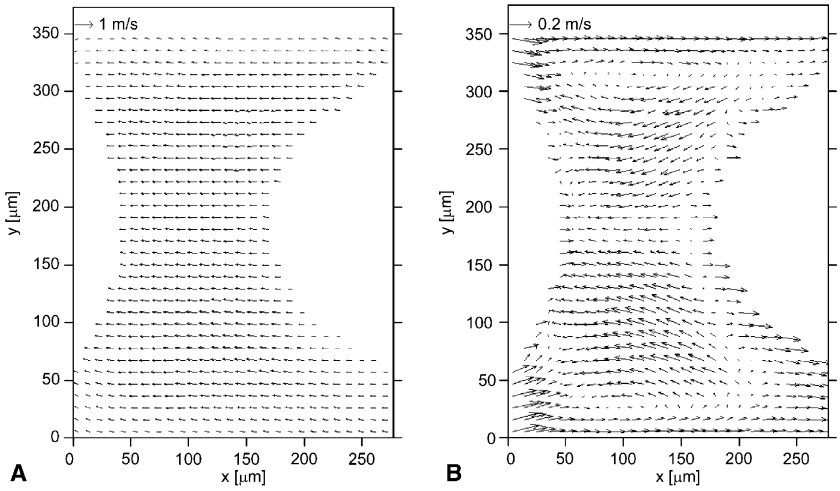

Fig. 10. Distribution of the absolute (A) and relative (B) velocities inside an ethanol plug.

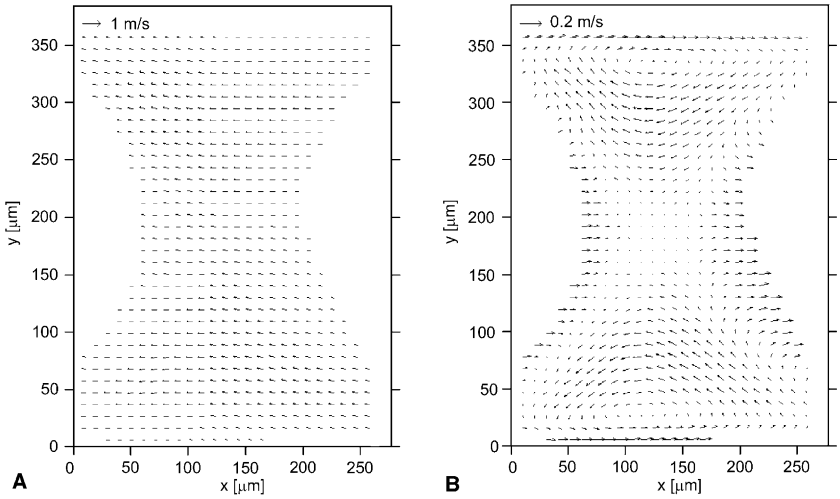

Fig. 11. Distribution of the absolute (A) and relative (B) velocities inside an aqueous glycerol plug.

A similar behavior can be found for a microchannel with a smaller hydraulic diameter of $D_h = 187.5$ µm. Using the same volumetric flow rates ($\dot{V}_L = 0.1$ ml/min, $\dot{V}_G = 1.0$ nml/min), the superficial velocities are increased to $j_L = 0.044$ m/s and $j_G = 0.44$ m/s, respectively. For this geometry the liquid Reynolds numbers are $Re_{L,water} = 9.15$, $Re_{L,eth} = 6.06$ and $Re_{L,glyc} = 5.00$. The gas phase Reynolds number is $Re_G = 5.39$ for all the analyzed fluid combinations. The average velocities are $v_{average} = 0.46$ m/s using water, 0.64 m/s in the ethanol plug and 0.43 m/s for the glycerol case, respectively.

The highest relative velocities were again measured in the ethanol case (Fig. 12B). The two conditions "water–nitrogen" (Fig. 12A) and "glycerol–nitrogen" (Fig. 12C) show similar characteristics, including low velocities at the center line and two stagnation points in the vicinity of the gas bubbles leading and trailing end.

In all the presented configurations, the gas bubble trailing end curve radius is found to be larger than the leading end curve radius. For the ethanol plug however, the leading edge is significantly more copped than in the two other configurations. This leads to an asymmetry of the two counter-rotating vortices in respect of the line perpendicular to the flow direction (see Fig. 13).

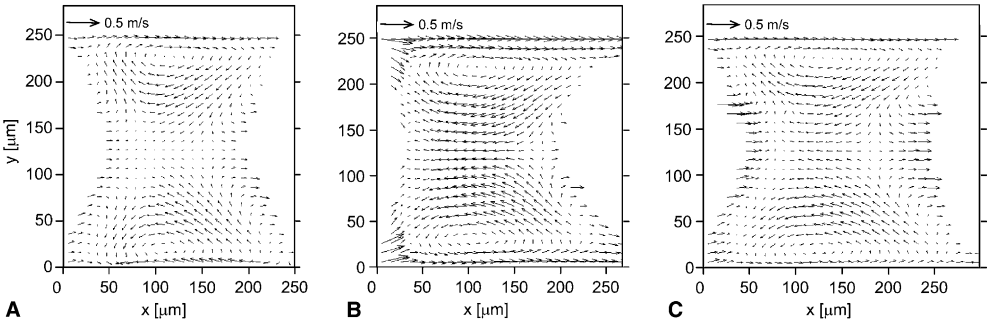

Fig. 12. Comparison of the relative velocities in a liquid plug of water (A), ethanol (B) and glycerol (C) for a microchannel with a hydraulic diameter of $D_h = 187.5$ μm.

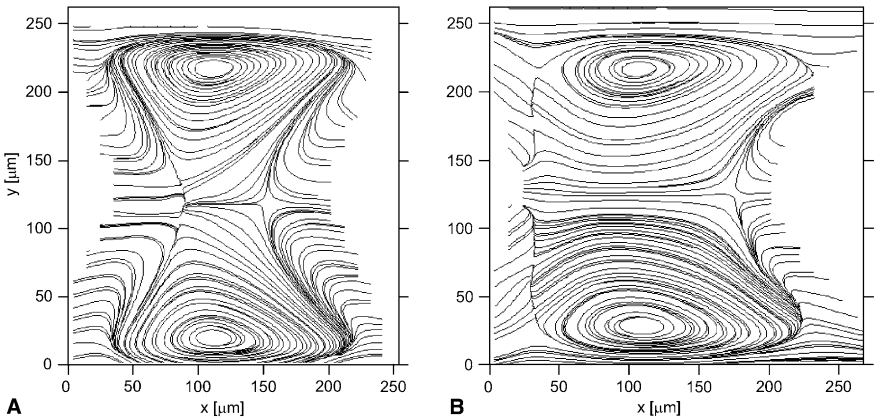

Fig. 13. Streamlines of the relative velocities for a microchannel with a hydraulic diameter $D_h = 187.5$ μm using water (A) and ethanol (B) as working fluid.

5. Conclusions

5.1. Flow pattern maps

Flow pattern maps for rectangular microchannels and a large variety of flow conditions and fluid combination are presented. The existing flow regime maps, where the transition boundaries are mostly plotted against the according gas and liquid superficial velocity are valid for a particular fluid combination only. Therefore a flow pattern map plotted against dimensionless numbers is presented. Even though only a few dimensionless numbers are used, the regime maps show good agreement for all the used fluids and hydraulic diameters. For the presented pattern map, the influence of the channel cross-section (in our case rectangular) and the material of the microchannel (silicon) were not taken into account and the temperature was not varied. The fluid properties as the viscosity, the density or the surface tension are strongly dependent on changes in temperature. Therefore the flow maps presented in Section 4.1 are valid only for room temperature.

The existing flow regime maps based on large scale pipe and channel flow are not capable to predict the flow pattern for two-phase flow in microchannels. The influence of the gravity, which is the main influence of the flow in macrochannels or large diameter pipes leads to wrong results. The ability of flow pattern maps based on experiments in microchannels to predict the correct flow regime is mainly dependent on the similarity of the cross-sectional channel shape and not on a similarity in hydraulic diameters. The flow pattern maps by Triplett et al. (1999) and Coleman and Garimella (1999) (semi-triangular and rectangular channel cross-section, respectively) predict an accurate flow pattern even for hydraulic diameters larger than the ones used in the present study by up to a factor 25. The prediction of Zhao and Bi (2001), Kawahara et al. (2002) and Coleman

and Garimella (1999) (circular channels) are insufficient even for hydraulic diameters of the same order of magnitude.

Microreactors are commonly designed for a specific chemical reaction. Taking into account that the void fraction, and therefore the flow pattern may change along the reaction path (gas release or consumption), an experimental verification of the flow properties is absolutely necessary for a new reactor design.

5.2. Liquid velocity distribution

A detailed study of the liquid velocity distribution in intermittent flows in microchannels is presented in this study. The influences of the liquid properties and the channel geometry is analyzed. The recirculation inside the liquid phase is shown to be affected by interfacial forces more than by the liquid viscosity. For all the presented configurations no remarkable mass transfer over the center line could be measured. Especially for catalytic gas–liquid reactions where the catalyst is applied at the reactor walls, this can be a relevant disadvantage. To enhance the mixing over the center line of a microreactor, geometrical adaptations are required in low Reynolds number flows. This can be meandering reactor channels or a static mixer (Wang et al., 2002).

References

Baker, O., 1954. Simultaneous flow of oil and gas. Oil Gas J. 53, 184–195.

Buckingham, E., 1914. On physically similar systems; illustrations of the use of dimensional equations. Phys. Rev. Lett. 4, 345–376.

Coleman, J.W., Garimella, S., 1999. Characterization of two-phase flow patterns in small diameter round and rectangular tubes. Int. J. Heat Mass Transfer 42, 2869–2881.

de Mas, N., Gunther, A., Schmidt, M.A., Jensen, K.F., 2003. Microfabricated multiphase reactors for the selective direct fluorination of aromatics. Ind. Eng. Chem. Res. 42, 698–710.

Ehrfeld, W., Hessel, V., Lowe, H., 2000. Microreactors. New Technology for Modern Chemistry. Wiley-VCH.

Kawahara, A., Chung, P.M.Y., Kawaji, M., 2002. Investigation of two-phase flow pattern, void fraction and pressure drop in a microchannel. Int. J. Multiphase Flow 28, 1411–1435.

Kolb, G., Hessel, V., 2004. Micro-structured reactors for gas phase reactions. Chem. Eng. J. 98, 1–38.

Losey, M.W., Schmidt, M.A., Jensen, K.F., 2001. Microfabricated multiphase packed-bed reactors: characterization of mass transfer and reactions. Ind. Eng. Chem. Res. 40, 2555–2562.

Meinhart, C.D., Wereley, S.T., Santiago, J.G., 1999. Piv measurements of a microchannel flow. Exp. Fluids 27, 414–419.

Santiago, J.G., Wereley, S.T., Meinhart, C.D., Beebe, D.J., Adrian, R.J., 1998. A particle image velocimetry system for microfluidics. Exp. Fluids 25, 316–319.

Triplett, K.A., Ghiaasiaan, S.M., Abdel-Khalik, S.I., Sadowski, D.L., 1999. Gas–liquid two-phase flow in microchannels—Part I: two-phase flow patterns. Int. J. Multiphase Flow 25, 377–394.

Wang, H.Z., Iovenitti, P., Harvey, E., Masood, S., 2002. Optimizing layout of obstacles for enhanced mixing *m* microchannels. Smart Mater. Struct. 11, 662–667.

Zhao, T.S., Bi, Q.C., 2001. Co-current air–water two-phase flow patterns in vertical triangular microchannels. Int. J. Multiphase Flow 27, 765–782.

Zlokarnik, M., 1983. Model scale-up in chemical-engineering. Chem. Ing. Tech. 55, 363–372.